Optimization analysis of the effects of the mounting configuration on surface shape of KDP crystal

Jian Shen[a,b], Zhigang Liu[a], Jianqiang Zhu*[a]
[a]Shanghai Institute of Optics and Fine Mechanics, No.390 Qinghe Rd, Jiading, Shanghai, China, 201800
[b]University of Chinese Academy of Sciences, Beijing, China, 100049

ABSTRACT

The deformation of KDP crystals caused by gravity and mounting force can induce the phase mismatch, resulting in the decrease of frequency conversion efficiency. Loading strips are used to reduce the distortion in some existing methods, but it is difficult to fabricate. In order to improve the surface shapes of KDP crystals, small loading plates are used instead of loading strips. The mounting configuration is analyzed by finite element methods (FEM) and the position of the loading plates is optimized by adaptive single-objective algorithm. The results show the effectiveness of the mounting configuration in reducing the gravitational sag of KDP crystals.

Keywords: mounting configuration, surface shape, KDP crystal, optimization

1. INTRODUCTION

Because of the excellent performance at frequency conversion, KDP crystals are widely used as frequency conversion optics in Inertial Confinement Fusion (ICF) devices, such as the National Ignition Facility (NIF) in the USA[1] and the Laser Megajoule (LMJ) in France[2]. Generally the optics in these ICF devices have the geometric property of a large ratio of apertures to thickness, which easily causes gravitational sag. The deformation caused by gravity leads to a departure from the phase-matching condition, eventually resulting in the decrease of frequency conversion efficiency[3,4,5].

Mounting the optics in appropriate way to minimize gravitational sag is one of the solutions to this problem. Various kinds of mounting configurations have been put forward and applied in ICF fields. C.E.Barker et al[6] and J.M.Auerbach et al[7] studied three types of boundary conditions: simple support all four corners, simple support all four edges and clamped support all four edges. R.L.Hibbard et al[8] designed a precision monolithic cell in which the optics was supported at the periphery. P.J.Wegner et al[9] mounted the optical components in a rigid mechanism with stainless steel. In O.Lubin's[10] scheme, the KDP plates were held at vertical edges with silicone seal. Y.Liang et al[11] proposed a torque mounting configuration where the external loads brought about the torque to mitigate the distortion and stress. R.Su et al[12] analyzed a kind of full periphery mounting configuration with adjusting function.

In previous work, the optical components are generally loaded at the periphery by means of mechanical mounts. And the loading forces are usually applied from long plates or strips, whose length is always nearly the same as the side length of the optics. But from the point of processing, it is difficult to machine a long plate when there are strict requirements for straightness, parallelism and roughness, which have influence on the distribution of forces. In this paper, short loading plates are used instead of loading strips in order to improve the surface shapes of KDP crystals and reduce the processing difficulty. The position of the loading plates is optimized numerically by adaptive single-objective algorithm and the mounting configuration is analyzed mechanically by finite element methods (FEM).

2. MOUNTING CONFIGURATION

The mounting configuration is shown in Figure 1. The optics has a plate structure with the dimensions of 350mm × 350mm × 10.5mm, supported on 5-millimeter-wide shim strips at all four edges of its bottom surface. Each edge has 4

*Corresponding author: jqzhu@mail.shcnc.ac.cn

2015 International Conference on Optical Instruments and Technology: Advanced Lasers and Applications, edited by Jianqiang Zhu, Chunqing Gao, Proc. of SPIE Vol. 9621, 96210N · © 2015 SPIE
CCC code: 0277-786X/15/$18 · doi: 10.1117/12.2191250

front loading plates and 2 side loading plates. The front loading plates axially (Z direction) squeeze the optics at the front loading regions, which are 5mm × 10mm squares at the edge of the top surface of the optics, and the side loading plates radially (X and Y direction) press the optics. The constraint screws are used to restrain the displacement in X and Y direction and the rotation around Z axis of the optics. Both the locking blocks and the shim strips are fixed to the frame. As required by optical demands, the angle between the normal (Z direction) and gravity is 45 °in YZ plane[12].

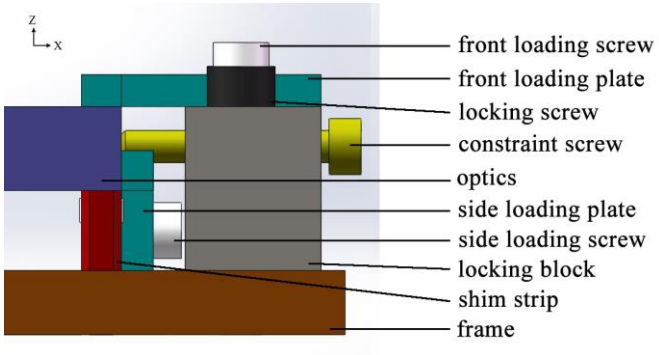

Figure 1. Mechanical mounting configuration for the optics.

3. THEORY AND METHODS

3.1 Mechanical analysis theory

According to the elastic mechanics theory, the deformation could be solved by the following equation

$$[K]\{\delta\} = \{F\}, \tag{1}$$

where $\{\delta\} = \{u \quad v \quad w\}^T$ is the deformation matrix, and u, v and w are the deformations in X,Y and Z directions respectively. $[K]$ is the stiffness matrix determined by the material. $\{F\}$ is the load matrix.

The strain could be obtained from the following geometric equation

$$\{\varepsilon\} = [B]\{\delta\}, \tag{2}$$

where $\{\varepsilon\} = \{\varepsilon_{xx} \quad \varepsilon_{yy} \quad \varepsilon_{zz} \quad \gamma_{yz} \quad \gamma_{xz} \quad \gamma_{xy}\}^T$ is the strain matrix, ε_{xx}, ε_{yy} and ε_{zz} are strains in X, Y and Z directions respectively, γ_{yz}, γ_{xz} and γ_{xy} are shear strains in YZ, XZ and XY planes respectively. $[B]$ is the geometric matrix defined as

$$[B] = \begin{bmatrix} \frac{\partial}{\partial x} & 0 & 0 & 0 & \frac{\partial}{\partial z} & \frac{\partial}{\partial y} \\ 0 & \frac{\partial}{\partial y} & 0 & \frac{\partial}{\partial z} & 0 & \frac{\partial}{\partial x} \\ 0 & 0 & \frac{\partial}{\partial z} & \frac{\partial}{\partial y} & \frac{\partial}{\partial x} & 0 \end{bmatrix}. \tag{3}$$

Based on the strain, the stress are then solved from the following physical equation

$$\{\sigma\} = [D]\{\varepsilon\}, \tag{4}$$

where $\{\sigma\} = \{\sigma_{xx} \quad \sigma_{yy} \quad \sigma_{zz} \quad \tau_{yz} \quad \tau_{xz} \quad \tau_{xy}\}^T$ is the stress matrix, σ_{xx}, σ_{yy} and σ_{zz} are stress in X, Y and Z directions respectively, τ_{yz}, τ_{xz} and τ_{xy} are shear stress in YZ, XZ and XY planes respectively. $[D]$ is the elastic

matrix representing the relationship between the strain and the stress. As the KDP crystal is a kind of anisotropic material, the constitutive relation is

$$\begin{Bmatrix} \sigma_{xx} \\ \sigma_{yy} \\ \sigma_{zz} \\ \tau_{yx} \\ \tau_{xz} \\ \tau_{xy} \end{Bmatrix} = \begin{bmatrix} D_{11} & D_{12} & D_{13} & 0 & 0 & 0 \\ D_{12} & D_{11} & D_{13} & 0 & 0 & 0 \\ D_{13} & D_{13} & D_{33} & 0 & 0 & 0 \\ 0 & 0 & 0 & D_{44} & 0 & 0 \\ 0 & 0 & 0 & 0 & D_{44} & 0 \\ 0 & 0 & 0 & 0 & 0 & D_{66} \end{bmatrix} \begin{Bmatrix} \varepsilon_{xx} \\ \varepsilon_{yy} \\ \varepsilon_{zz} \\ 2\gamma_{yx} \\ 2\gamma_{xz} \\ 2\gamma_{xy} \end{Bmatrix}, \tag{5}$$

where $D_{11} = 71.2$, $D_{12} = -5.0$, $D_{13} = 14.1$, $D_{33} = 56.8$, $D_{44} = 12.6$, $D_{66} = 6.22$ (in units of GPa)[10].

The deformation and the stress of KDP crystal in the mounting configuration can be solved from the above equations. However, it is difficult to obtain the analytical solution. One alternative is calculating the numerical solution by means of finite element methods, in which the solid structure is divided into discrete nodes and elements. The stress and deformation of each node are calculated and the global solution of the structure is obtained by integrating the local solutions.

3.2 Finite element model

The model of the mounting configuration is established and analyzed by the finite element package ANSYS. In order to facilitate the modeling and analysis, some reasonable simplifications are processed. The finite element model mainly consists of the optics and the shim strips, and both are solid modeled and meshed with 65638 nodes and 12705 elements in total. The optics is made of KDP crystal. The external loads, in the form of pressure, are applied on the loading region at the top and side surfaces of the optics. The displacement in X and Y direction and the rotation around Z axis of the optics is constrained. The optics contacts with the shim strips at the supporting region, where the contact pairs are constructed. The bottom surfaces of the shim strips are fixed. Gravity acts on the model with a 45 degree angle to the normal in YZ plane. The material properties are listed in Table 1 and the finite element model of the mounting system is shown in Figure 2.

Table 1. Material properties.

Material	Young's Modulus (Pa)	Poisson's Ratio	Density (kg/m^3)
KDP			2340
steel	2.0×10^{11}	0.3	7850

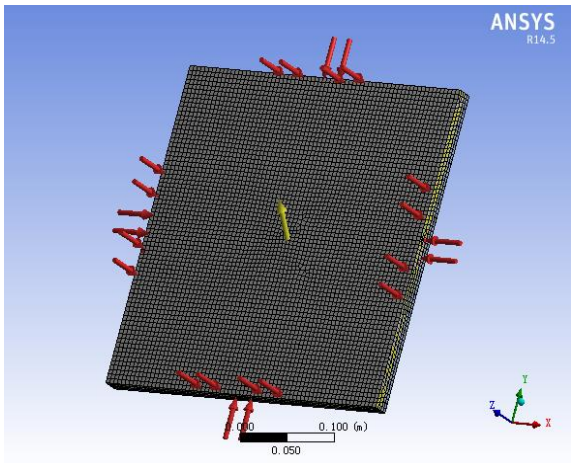

Figure 2. Finite element model of the mounting configuration.

3.3 Optimization method

Optimization method is applied to search for the optimal parameters of the system. The position of the loading plates is optimized by adaptive single-objective algorithm, which is mainly based on Nonlinear Programming by Quadratic Lagrangian (NLPQL) method. The NLPQL method is a kind of Sequential Quadratic Programming (SQP) method, which expands the objective function into the second Taylor expansion and linearizes the constraints, turning the nonlinear problem to a quadratic programming problem. The general form of constrained nonlinear programming problem can be described as[13,14]

$$\begin{cases} \min f(\mathbf{x}) & \mathbf{x} \in R^N \\ s.t.\ c_i(\mathbf{x}) & i = 1, 2, \ldots, m \end{cases}, \tag{6}$$

where $\mathbf{x} = [x_1, x_2, \cdots x_n]^T$ is the variable, $f(\mathbf{x})$ is the objective function and $c_i(\mathbf{x})$ is the constraints.

The above optimization problem can be summarized as a quadratic programming problem

$$\begin{cases} \min QP(s) = \left[\nabla f(\mathbf{x}^{(k)})\right]^T s + \dfrac{1}{2} s^T \mathbf{B}^{(k)} s \\ \quad s.t.\ c_i(\mathbf{x}^{(k)}) + \left[\nabla c_i(\mathbf{x}^{(k)})\right]^T s = 0 \qquad i = 1, 2, \ldots, m \end{cases}, \tag{7}$$

where s is the search direction, $\mathbf{B}^{(k)}$ is the approximation of Hessen matrix, $\alpha_k s^{(k)} = \mathbf{x}^{(k+1)} - \mathbf{x}^{(k)}$ and α_k is the step coefficient.

The solving steps are as follows:

(1) Selecting the appropriate initial point $\mathbf{x}^{(0)}$, α_0, $\mathbf{B}^{(0)}$ and tolerance ε_1.

(2) Solving the quadratic programming problem QP, identifying new Lagrange multiplier vector $\lambda^{(k+1)}$ and the search direction $s^{(k)}$.

(3) Identifying step coefficient α_k and calculating new iterative point $\mathbf{x}^{(k+1)} = \mathbf{x}^{(k)} + \alpha_k s^{(k)}$.

(4) Judging whether it meets the convergence criteria or not. If so, stop the iteration; if not, go to step 5.

(5) Modifying $\mathbf{B}^{(k)}$ and letting $k = k + 1$, then returning to step 2.

3.4 Parameter settings for optimization

In the mounting configuration, the parameter settings are shown in Figure 3. Considering the symmetry of the structure, 4 parameters are needed on the front surface and 1 parameter on each side surface. X1, X2, Y1, and Y2 are the dimension parameters on the front surface which determine the front loading regions, and d1~d4 are on side surfaces determining the 4 side loading regions respectively. So there are 8 parameters in all.

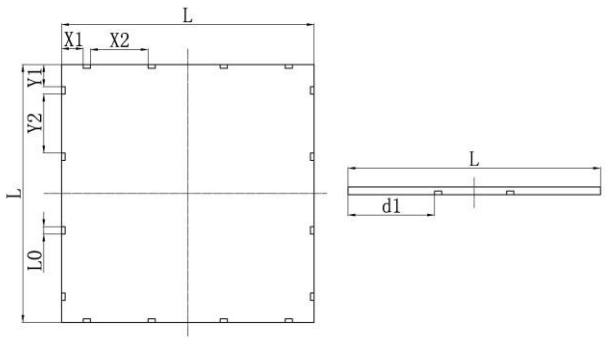

Figure 3. Parameter settings for optimization.

According to the design requirements of structure, these parameters need to meet the following conditions

$$\begin{cases} 0 \le X1 + X2 \le \dfrac{1}{2} L - 2L_0 \\ 0 \le Y1 + Y2 \le \dfrac{1}{2} L - 2L_0 \\ 0 \le d_i \le \dfrac{1}{2} L - L_0, \quad i = 1,2,3,4 \end{cases}, \tag{8}$$

where L is the side length of the optics and L_0 is the length of each loading region.

4. RESULTS AND DISCUSSION

4.1 Optimization of the structure

Based on the design requirements shown in Section 3.4 and preliminary sampling test, the initial scopes of the parameters are set as Table2. By calculation the parameters converge to a small neighborhood of the optimal values. The convergence process of the parameters is shown in Figure 4 and the convergence values are shown in Table 3. The design values are rounded-off values from the convergence solution for the convenience of designing and processing.

Table 2. Initial scopes of the parameters.

Parameter	Lower bound (mm)	Upper bound (mm)
X1, Y1	70	120
X2, Y2	10	30
d1~d4	130	160

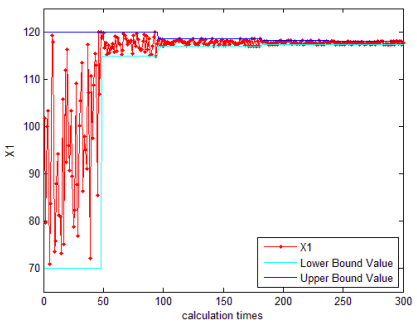

(a) X1

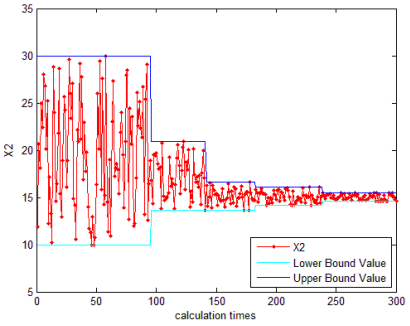

(b) X2

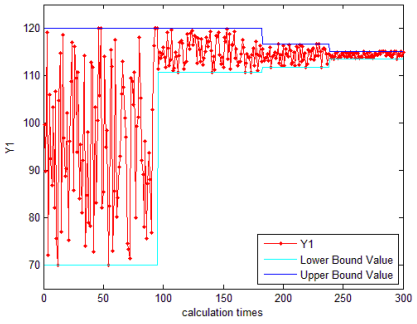

(c) Y1

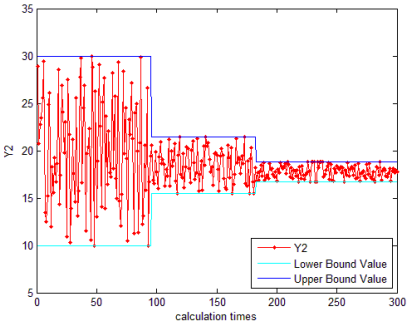

(d) Y2

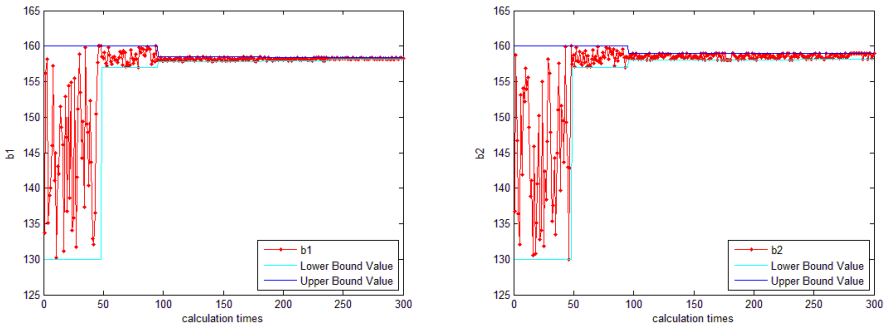

(e) b1 (f) b2

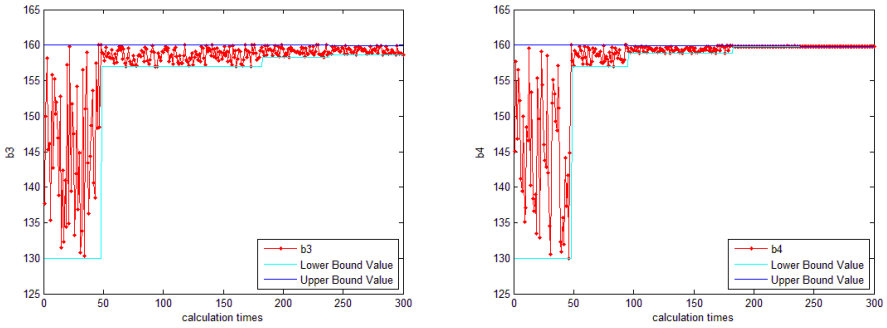

(g) b3 (h) b4

Figure 4. The convergence process of each parameter.

Table 3. Optimized values of the parameters.

Parameter	Lower bound (mm)	Lower bound (mm)	Optimal value (mm)	Design value (mm)
X1	117.3032	118.0767	117.3556	118
X2	14.6473	15.4976	14.9733	15
Y1	113.5778	115.0600	114.1166	114
Y2	16.7111	18.8219	18.2428	18
d1	158.1296	158.3685	158.2350	160
d2	158.1366	159.0339	159.0237	160
d3	158.6430	159.9234	158.7406	160
d4	159.7781	159.8256	159.8045	160

4.2 Deformation of the KDP plate

According to the results of optimization in Section 4.1, the structure is redesigned with the optimized parameters that the loading plates are placed in the optimal position. And the optimized structure is then analyzed mechanically. Since the aperture size of the laser beam studied here is 300mm × 300mm, only the deformation and stress of the optics within this pupil area are studied.

Due to the influence of the gravity, a sag in –Z direction appears in the center of the optics, as shown in Figure 6(a). When the external loads are applied, the deformation of the optics changes, as shown in Figure 6(b). In order to evaluate

the data, the root mean square (RMS) value is introduced. The deformation studied here is the RMS value of the nodes within the pupil area, representing the general deformation of the area.

When the external loads increase from 0 to 0.30MPa, the center of the KDP plate deforms in +Z direction, the sag disappears and the surface becomes smoother. The RMS value of the deformation consequently decreases from 1.46μm to 0.637μm.

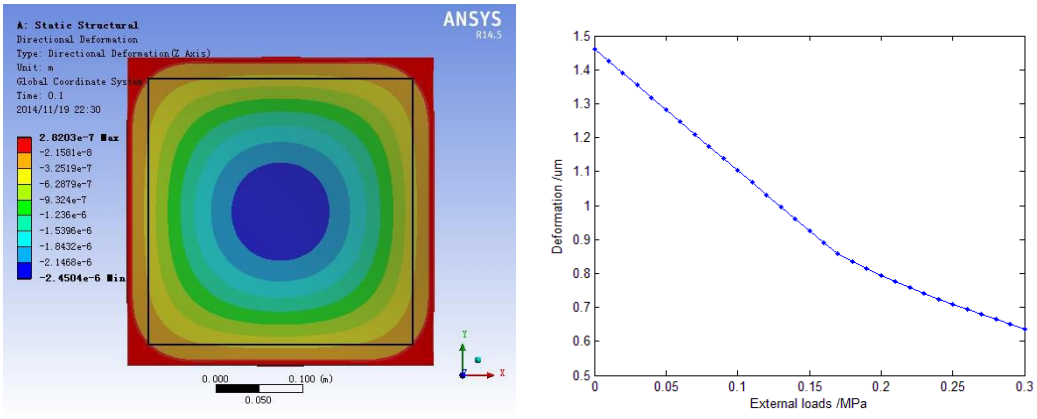

(a) (b)

Figure 5. Effects of the external loads on the deformation of the optics. (a) The initial surface shape of the KDP plate. The black wire frame here represents the pupil area. (b) The deformation changes with the external loads.

4.3 Stress of the KDP plate

The stress studied here are the RMS value of the nodes within the pupil area, representing the general stress of the area. The stress within the pupil area are mainly caused by deformation. The stress near the loading regions are mainly caused by external loads and much larger in value than the former one.

The external loads changes the stress distribution of the KDP plates. When the external loads increase from 0 to 0.20MPa, the deformation within the pupil area decreases, and the stress decrease from 0.0323MPa to 0.0213MPa consequently. When the external loads are larger than 0.20MPa, the influence scope of the external loads expands to the pupil area, increasing the general stress within this area. Figure 7 shows the effects of the external loads on the stress of the optics.

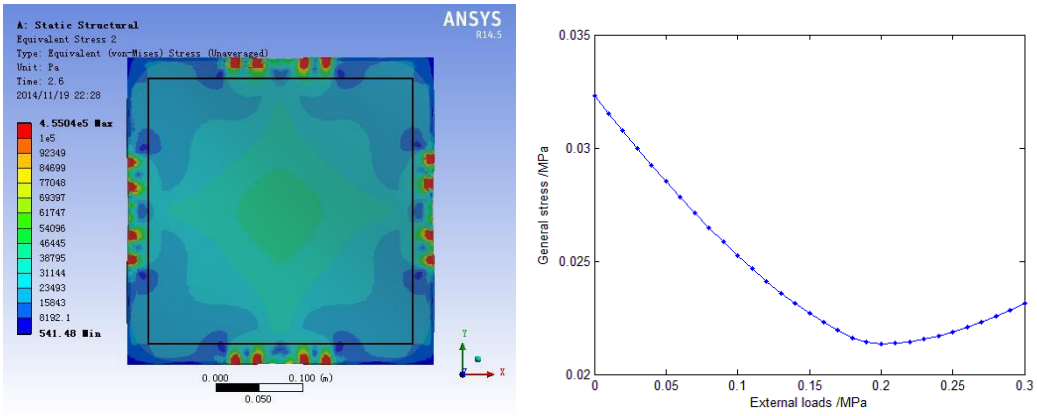

(a) (b)

Figure 6. Effects of the external loads on the stress of the optics. (a) The stress distribution of 0.20MPa. The black wire frame here represents the pupil area. (b) The stress change with the external loads.

5. CONCLUSION

In order to decrease the deformation and stress caused by gravity, the mounting configuration with short loading plates is proposed. The position of the loading plates is numerically optimized by single-objective algorithm and the structure is mechanically analyzed with finite element method. The results show that, each of the loading plates has its own optimal position. In other words, the mounting forces should be applied on their best locations, so that the quality of the surface shape can be optimal. When the external loads increase within a certain range, the deformation and stress of the optics can be reduced effectively.

REFERENCES

[1] Burkhart S C, Bliss E, Di Nicola P, et al., "National Ignition Facility system alignment," Applied Optics 50(8), 1136-1157(2011).

[2] Fleurot N, Cavailler C, Bourgade J L., "The Laser Megajoule (LMJ) Project dedicated to inertial confinement fusion: Development and construction status," Fusion Engineering and Design 74(1), 147-154(2005).

[3] Li K, Zhang B., "Analysis of broadband third harmonic generation with non-collinear angular dispersion in KDP crystals," Optics Communications 281(8), 2271-2278(2008).

[4] Li K, Jia H, Wang C, et al., "Theory and experiment analysis of factors affecting THG efficiency for the TIL prototype laser facility," Optik-International Journal for Light and Electron Optics 120(1), 1-8(2009).

[5] Auerbach J M, Wegner P J, Couture S A, et al., "Modeling of frequency doubling and tripling with measured crystal spatial refractive-index nonuniformities," Applied optics 40(9), 1404-1411(2001).

[6] Barker C E, Auerbach J M, Adams C H, et al., "National Ignition Facility frequency converter development," Second International Conference on Solid State Lasers for Application to ICF, International Society for Optics and Photonics, 197-202(1997).

[7] Auerbach J M, Barker C E, Couture S A, et al., "Modeling of frequency doubling and tripling with converter refractive index spatial nonuniformities due to gravitational sag," Third International Conference on Solid State Lasers for Application to Inertial Confinement Fusion, 472-479(1999).

[8] Hibbard R L., "Design of precision mounts for optimizing the conversion efficiency of KDP crystals for the National Ignition Facility," Lawrence Livermore National Lab., (1998).

[9] Wegner P J, Auerbach J M, Barker C E, et al., "Frequency converter development for the National Ignition Facility," Third International Conference on Solid State Lasers for Application to Inertial Confinement Fusion, International Society for Optics and Photonics, 392-405(1999).

[10] Lubin O, Gouedard C., "Modeling of the effects of KDP crystal gravity sag on third-harmonic generation," Third International Conference on Solid State Lasers for Application to Inertial Confinement Fusion, International Society for Optics and Photonics, 802-808(1999).

[11] Liang Y, Su R, Liu H, et al., "Analysis of torque mounting configuration for nonlinear optics with large aperture," Optics & Laser Technology 58, 185-193(2014).

[12] Su R, Liu H, Liang Y, et al., "Analysis of adjusting effects of mounting force on frequency conversion of mounted nonlinear optics," Applied optics 53(2), 283-290(2014).

[13] Jiang W, Gao Q, Zhang M, et al., "Optimization of electronic control unit pump parameters based on NLPQL," Vehicle engine 3, 25-28(2011)

[14] Schittkowski K., "NLPQL: A FORTRAN subroutine solving constrained nonlinear programming problems," Annals of operations research 5(2), 485-500(1986).